Disentangling intrinsic and extrinsic Gilbert damping

Zhengmeng Xu, Kai Zhang, and J. Li*
International Center for Quantum Materials, School of Physics, Peking University, Beijing 100871, China

(Received 5 August 2021; revised 24 October 2021; accepted 18 November 2021; published 6 December 2021)

Magnetic damping is of great interest due to its importance in magnetization switching and dynamics. Here, we report the quantitative disentanglement of intrinsic and extrinsic Gilbert damping in epitaxial Fe thin films. Both intrinsic damping and two-magnon scattering (TMS) make significant contributions to the total Gilbert damping, leading to an enhanced total damping at low temperature. Our result suggests the correlation between interfacial magnetic anisotropy and TMS.

DOI: 10.1103/PhysRevB.104.224404

I. INTRODUCTION

Magnetic damping determines the magnetic relaxation rate in magnetization dynamics, which is usually characterized by the phenomenological Gilbert damping parameter α_G in the Landau-Lifshitz-Gilbert equation [1]. Minimizing α_G is of critical importance for magnonic devices of high-speed and low-power dissipation [2–4]. Hitherto, great efforts have been dedicated to quantitatively estimate α_G in metallic ferromagnets, e.g., the breathing Fermi-surface, torque correlation, and scattering models [5–7], aiming to exploit the damping mechanisms and engineer α_G [8]. In Kamberský's [5] torque correlation model, it is predicted that intrinsic Gilbert damping is governed by intraband transition (conductivity-like behavior) at low temperature and by interband transition (resistivitylike behavior) at high temperature [6]. Such nonmonotonic temperature dependence of α_G has been observed in three-dimensional magnetic metals [6,9], demonstrating the critical role of spin-orbit coupling and electron-phonon scattering in magnetic relaxation processes. In addition to the intrinsic damping, there exist several pervasive extrinsic damping mechanisms, e.g., two-magnon scattering (TMS) [10,11], eddy-current damping [12,13], radiative damping [14], and interfacial contributions [15]. Among these extrinsic contributions, TMS damping can be extracted via angular-dependent α_G measurements [16]. However, this approach would become impracticable with the presence of anisotropic Gilbert damping [17]. Meanwhile, the extractions of eddy-current and radiative damping usually rely on numerical calculations [3] rather than direct measurements. As a result, the interplay between intrinsic and pervasive extrinsic damping results in a substantial obstacle to quantitative investigation of the various damping mechanisms [18]. Therefore, from both fundamental and technological interests, it is urgent to have an effective experimental method to disentangle the various damping mechanisms and determine the intrinsic Gilbert damping.

In this paper, we report thickness-dependent α_G measurements in epitaxial Fe thin films. Intrinsic and extrinsic Gilbert damping are disentangled in the quantitative manner. The temperature dependences of intrinsic Gilbert and TMS damping are revealed, which result in an enhanced α_G at low temperature. The correlation between the interfacial fourfold anisotropy and TMS damping is revealed as well. Our result manifests the thickness-dependent α_G measurement as an effective method to quantitatively explore the various damping mechanisms.

II. SAMPLES AND EXPERIMENTS

The samples were fabricated in an ultrahigh vacuum chamber with a base pressure of 2×10^{-10} Torr. The MgO(001) substrate was annealed at 600 °C for 10 h. Then Fe films of different thicknesses were grown epitaxially on MgO(001) substrates at room temperature, succeeded by a 3-nm-thick MgO layer as the protection layer. Epitaxial Fe films were examined by x-ray diffraction (XRD) and x-ray reflectivity (XRR). Figure 1(a) shows the XRD spectrum of Fe thin film on a log scale; two diffraction peaks were found for MgO (002) and Fe (002). The XRR spectrum was fitted to obtain the thickness (5 nm) and surface roughness (0.3 nm) [Fig. 1(b)]. Such XRD and XRR spectra confirm the single crystallinity and quality of the epitaxial Fe films.

The samples were patterned into a standard Hall bar with a length of $L = 4$ mm and a width of $w = 100\,\mu$m by optical lithography and ion beam etching. An electrical current (0.1 mA) flowed along the Fe [100] direction. The planar Hall effect (PHE) was measured in a physical property measurement system (Quantum Design PPMS-9T system) with a rotatable sample stage. A static magnetic field was kept in the film plane during PHE measurements. The temperature dependence of the Fe film resistivity was also recorded [Fig. 1(c)].

Frequency-dependent ferromagnetic resonance (FMR) was measured using a coplanar waveguide (CPW) transmission setup. Samples were placed face down over the signal line of the CPW affixed at one end of a custom variable temperature insert, inserting into a Cryogenic Ltd cryogen-free

*Corresponding author: jiali83@pku.edu.cn

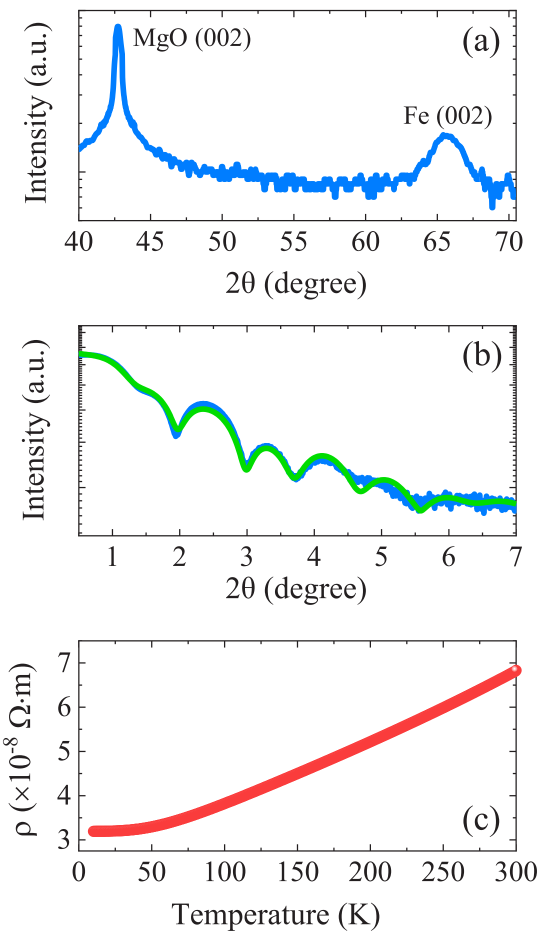

FIG. 1. (a) X-ray diffraction (XRD) spectrum and (b) x-ray reflectivity (XRR) spectrum (blue line) with fitting curve (green line) of the MgO(001)/Fe(5 nm)/MgO sample. (c) Temperature-dependent resistivity of the MgO(001)/Fe(5 nm)/MgO sample.

vector magnet. FMR signals were probed by vector network analyzer through S_21 transmission data at various magnetic fields within the temperature range between 10 and 300 K.

III. RESULTS AND DISCUSSION

A. Damping mechanisms in magnetic thin films

The total Gilbert damping α_G consists of intrinsic and extrinsic damping contributions [8], wherein the latter is usually caused by TMS, eddy-current and radiative damping, and interfacial contributions such as interfacial spin loss. Both intrinsic and extrinsic damping mechanisms are thickness dependent.

Intrinsic Gilbert damping may comprise the bulk contribution α_G^{bulk} and interface contribution α_G^{inter}. Here, α_G^{bulk} is an intrinsic property of a bulk magnetic material which is independent of the film thickness. On the contrary, the interface contributions including interfacial spin loss [15], interfacial isotropic scattering [19], and interfacial inhomogeneous magnetization states [20] are thickness dependent. Phenomenologically, the interface contribution α_G^{inter} is inverse in the film thickness d_{Fe} ($\alpha_G^{\text{inter}} = \beta_{\text{inter}}/d_{\text{Fe}}$) with the coefficient β_{inter} [19].

TMS is caused by the scattering centers for magnon scattering. In high-quality single-crystalline thin film, the scattering centers are present at the interfaces with respect to the ultralow density of scattering centers in the bulk of the film, as specified in the literature [16,18]. Hence, TMS damping α_{TMS} is quadratic in $1/d_{\text{Fe}}$ ($\alpha_{\text{TMS}} = \beta_{\text{TMS}}/d_{\text{Fe}}^2$), where β_{TMS} is the coefficient of TMS damping, and d_{Fe} is the Fe film thickness [18,21].

In a ferromagnetic conductor, any change in the magnetization induces eddy currents, resisting the magnetization dynamics which provides a damping mechanism [12]. Eddy-current damping α_{eddy} is quadratically proportional to the film thickness ($\alpha_{\text{eddy}} = \beta_{\text{eddy}} d_{\text{Fe}}^2$) [9,22]. The coefficient of $\beta_{\text{eddy}} = \gamma\mu_0^2 M_s \sigma/12$ is proportional to the conductivity σ, as well as the saturation magnetization $\mu_0 M_s$. Thus, α_{eddy} is expected to be effective for the thick film.

In CPW-based FMR experiments, the inductive coupling between the dynamic magnetization and the signal line of the CPW carries the energy out of the sample, leading to radiative damping α_{rad} [3]. Here, α_{rad} scales linearly with the film thickness ($\alpha_{\text{rad}} = \beta_{\text{rad}} d_{\text{Fe}}$) [14]. The coefficient of $\beta_{\text{rad}} = \eta\gamma\mu_0^2 M_s l/2Z_0 W$ is proportional to sample length l and inversely proportional to the CPW impedance Z_0 (50 Ω) as well as the width of the signal line W. Here, η is a dimensionless parameter accounting for the dynamic magnetization profile in the sample. For ultrathin films, α_{rad} is usually negligible.

The total damping α_G is given approximately by the sum of the damping mechanisms as

$$\alpha_G = \alpha_G^{\text{bulk}} + \frac{\beta_{\text{inter}}}{d_{\text{Fe}}} + \frac{\beta_{\text{TMS}}}{d_{\text{Fe}}^2} + \beta_{\text{rad}} d_{\text{Fe}} + \beta_{\text{eddy}} d_{\text{Fe}}^2. \quad (1)$$

Hence, disentanglement of the various damping mechanisms is achievable via a thickness-dependent measurement of α_G.

B. Disentanglement of intrinsic and extrinsic damping

To extract α_G, FMR signals were detected by measuring the real part of the S_{21} transmission parameter as a function of in-plane magnetic field H [Fig. 2(a)]. Figure 2(b) shows typical $S_{21}(H)$ data of the MgO(001)/Fe(3.3 nm)/MgO sample with H along the Fe [100] direction (microwave frequency $f = 12$ GHz). The change in $S_{21}(H)$ data due to FMR is fitted with a combination of symmetric and antisymmetric Lorentzian curves [3]:

$$V(H) = V_{\text{sym}} \frac{(\Delta H)^2}{(H - H_{\text{res}})^2 + (\Delta H)^2} + V_{\text{asym}} \frac{-2\Delta H (H - H_{\text{res}})}{(H - H_{\text{res}})^2 + (\Delta H)^2}, \quad (2)$$

where V_{sym} and V_{asym} are the amplitudes of symmetric and antisymmetric curves, respectively. Here, H_{res} is the resonance field, and ΔH is the linewidth corresponding to the half width at half maximum. The obtained ΔH scales linearly with f, as described by

$$\Delta H = \Delta H_0 + \frac{2\pi f \alpha_G}{\gamma}, \quad (3)$$

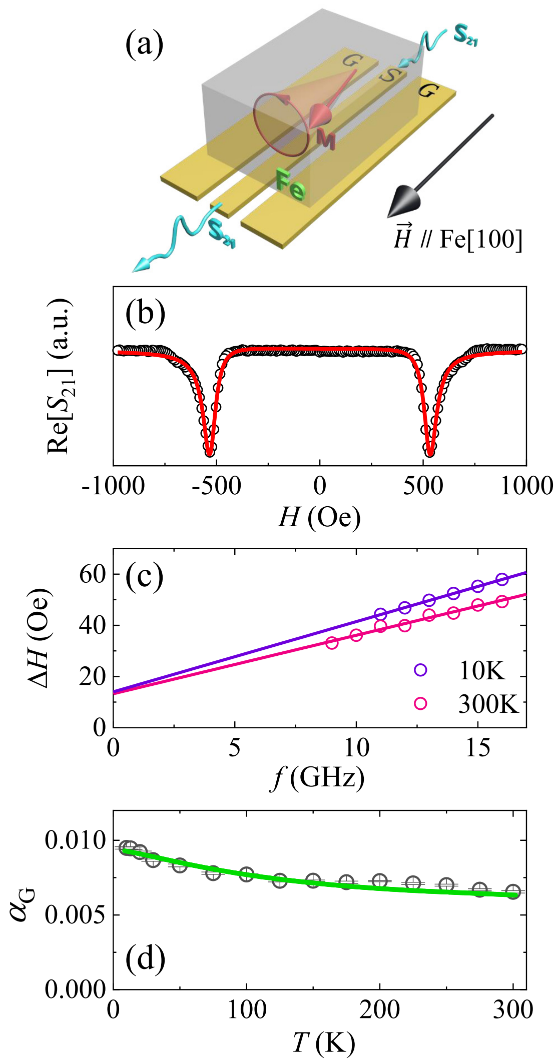

FIG. 2. (a) Schematic of the ferromagnetic resonance (FMR) measurements [MgO(001)/Fe(3.3 nm)/MgO sample]. (b) Typical $S_{21}(H)$ data at $f = 12$ GHz are fitted with Eq. (2) to extract ΔH. (c) The obtained ΔH is plotted against f at $T = 300$ and 10 K. The linear fitting with Eq. (3) provides α_G at different temperatures. (d) The temperature dependence of α_G is well described by Eq. (4).

where α_G is the Gilbert damping parameter, and γ is the gyromagnetic ratio. Here, ΔH_0 is the inhomogeneous linewidth broadening caused by long-range magnetic inhomogeneity. The linear fitting with Eq. (3) yields a Gilbert damping parameter of $\alpha_G \approx 0.006$ at $T = 300$ K, coincident with the reported values [23,24].

According to the linear fitting shown in Fig. 2(c), ΔH_0 is temperature independent, while α_G (the slope of the linear fitting) is apparently enhanced at low temperature. Figure 2(d) presents the temperature evolution of α_G, which validates the increase of α_G at low temperature, in agreement with the literature [9]. Phenomenologically, the temperature dependence of α_G can be fitted with a combination of the conductivitylike and resistivitylike terms [9]:

$$\alpha_G = \alpha_\sigma \frac{\sigma(T)}{\sigma(300\text{ K})} + \alpha_\rho \frac{\rho(T)}{\rho(300\text{ K})}, \tag{4}$$

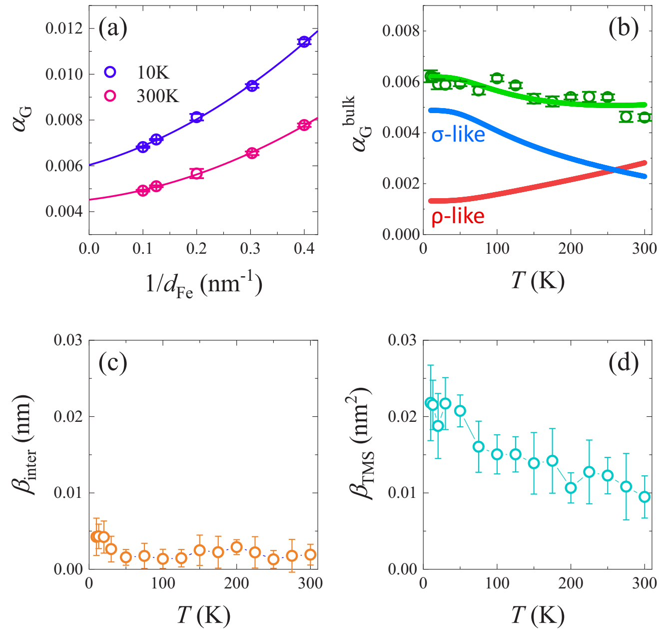

FIG. 3. (a) The thickness dependence of α_G at $T = 10$ and 300 K. Different damping mechanisms can be disentangled via the fitting with Eq. (1). (b) The temperature dependence of α_G^{int} is effectively described by a combination of conductivitylike and resistivitylike terms. (c) The coefficient β_{inter} of interfacial contributions is temperature independent in approximation. (d) The coefficient β_{TMS} of two-magnon scattering (TMS) damping is enhanced at low temperature.

where $\sigma(T)$ and $\rho(T)$ are the temperature-dependent conductivity and resistivity for the same film thickness, respectively. Here, α_σ and α_ρ are the fitting parameters to characterize the conductivitylike and resistivitylike contributions to α_G [6]. This fitting gives the ratio of $\alpha_\sigma/\alpha_\rho = 1.5$ [Fig. 2(d)], indicating that the conductivitylike contribution is dominative and gives rise to the α_G enhancement at low temperature.

For the sake of a quantitative understanding of this phenomenon, the disentanglement of the various damping mechanisms is demanded. Figure 3(a) depicts the thickness dependence of α_G at $T = 10$ and 300 K. Apparently, α_G is not a constant vs d_{Fe}, indicating the emergence of the extrinsic damping contributions. The various damping mechanisms are disentangled via the fitting with Eq. (1) [Fig. 3(a)], wherein the intercepts at $1/d_{Fe} = 0\,\text{nm}^{-1}$ quantify the bulk contribution of intrinsic Gilbert damping α_G^{bulk}. A significant contribution of TMS (β_{TMS}) is observed [Fig. 3(d)] in addition to α_G^{bulk} [Fig. 3(b)]. Meanwhile, a small interface contribution β_{inter} is revealed, which is temperature independent in approximation [Fig. 3(c)]. In addition, the quantitative fitting reveals the negligible contributions of eddy-current damping α_{eddy} and radiative damping α_{rad}, which are due to the ultrathin film thickness of epitaxial Fe [20]. It is worth noting that α_G^{bulk} and β_{TMS} are both enhanced at low temperature. Here, β_{TMS} is pronounced for ultrathin films and becomes negligible for thick films [9]. The temperature dependence of α_G^{bulk} is fitted with Eq. (4), producing the ratio of $\alpha_\sigma/\alpha_\rho = 0.8$ [Fig. 3(b)]. Accordingly, the conductivitylike contribution (intraband transition) dominates Gilbert damping at low temperature, while the resistivitylike contribution (interband transition) becomes dominative when adjacent to room temperature. Therefore, the intraband transition is an effective contribution to intrinsic Gilbert damping in Fe and gives rise to the $\alpha_G^{\rm bulk}$ enhancement at low temperature.

In addition, the α_G enhancement at low temperature is also partially ascribed to the increase of TMS damping at low temperature [Fig. 3(d)]. In ultrathin films, the uniform magnetization precession is expected in FMR mode. However, the presence of interfacial magnetic anisotropy could lead to the short wavelength magnons at the interfaces, contributing to TMS. Interfacial magnetic anisotropy thus plays a key role in TMS damping. To comprehend the increase of TMS damping at low temperature, we systematically studied the in-plane magnetic anisotropy of MgO(001)/Fe samples, with thickness and temperature dependence.

C. Interfacial fourfold magnetic anisotropy

It is well known that the body-centered cubic crystalline structure of the epitaxial Fe film on MgO(001) leads to an in-plane fourfold magnetic anisotropy [25]. Meanwhile, perpendicular magnetic anisotropy is absent in the MgO(001)/Fe system, thus is excluded in the following discussion. The in-plane magnetic anisotropy of Fe films is determined via the conventional balancing torque method [26]. The azimuthal directions of the external magnetic field H (ϕ_H) and Fe magnetization (ϕ_M) are required for the quantitative determination of magnetic anisotropy. Here, ϕ_M can be measured via PHE, which is expressed as $R_{xy} = \Delta R \sin 2\phi_M$ [27]. The transverse resistance R_xy depends on ϕ_M with respect to the current direction [Fig. 4(a)]. Here, ΔR characterizes the magnitude of PHE.

For a magnetic thin film with uniaxial anisotropy K_2 and fourfold anisotropy K_4, the balancing torque equation can be written as [25]

$$\tau(\phi_M) = H \sin(\phi_H - \phi_M) = -\tfrac{1}{2}H_2 \sin 2\phi_M - \tfrac{1}{4}H_4 \sin 4\phi_M. \quad (5)$$

Here, $H_2 = 2K_2/M_s$ and $H_4 = 2K_4/M_s$ are the uniaxial and fourfold anisotropic fields. Here, M_s is the saturation magnetization, and H_2 and H_4 can be determined quantitatively via the fitting with Eq. (5).

Figure 4(b) shows the ϕ_H-dependent R_xy of the MgO(001)/Fe(2 nm)/MgO sample ($H = 500$ Oe) at room temperature. Apparently, the ϕ_H-dependent R_xy deviates from the $\sin 2\phi_H$ curve due to the magnetic anisotropy of single-crystalline Fe film. We calculated ϕ_M at different ϕ_H according to $\phi_M = \sin^{-1}(R_{xy}/\Delta R)/2$, as well as the torque moment $\tau(\phi_M)$ [Fig. 4(c)]. According to the quantitative fitting with Eq. (5), the uniaxial anisotropic field of $H_2 = 11$ Oe and fourfold anisotropic field of $H_4 = 207$ Oe were obtained. The strength of H_4 is consistent with the reported value in the literature [25,26]; the small H_2 is usually attributed to the step surface of the MgO(001) substrate [26]. The obtained H_4 is independent of the strength of H [Fig. 4(d)], revealing the intrinsic nature of the obtained H_4.

Phenomenologically, H_4 of single-crystalline Fe thin film can be partitioned into the bulk contribution and surface contribution ($H_4 = H_4^b + H_4^s/d_{\rm Fe}$) [28]. The bulk contribution

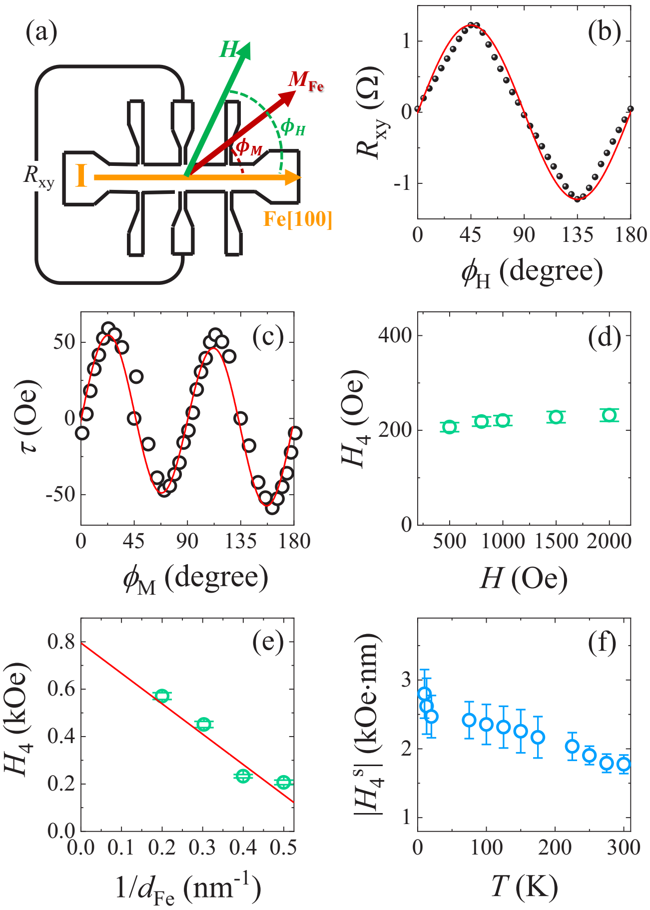

FIG. 4. (a) Schematic of planar Hall effect (PHE) measurements. (b) The ϕ_H-dependent R_xy of the MgO(001)/Fe(2 nm)/MgO sample ($H = 500$ Oe) at room temperature. Red curve plots the PHE expression of $\Delta R \sin 2\phi_H$. (c) The torque moments as a function of $\phi_{\rm M}$, fitted with Eq. (5). (d) H_4 is independent of the static magnetic field H. (e) The linear fitting of $1/d_{\rm Fe}$-dependent H_4 ($H_4 = H_4^b + H_4^s/d_{\rm Fe}$) provides H_4^b (the intercept) and H_4^s (the slope) at room temperature. (f) The magnitude of H_4^s is enhanced at low temperature.

(H_4^b) is independent of the Fe film thickness $d_{\rm Fe}$, while the surface contribution ($H_4^s/d_{\rm Fe}$) is inverse in $d_{\rm Fe}$. Therefore, H_4^b and H_4^s can be determined through the thickness dependence of H_4, as shown in Fig. 4(e). The positive H_4^b (the intercept of the linear fitting) reveals the intrinsic fourfold magnetic anisotropy of single-crystalline Fe films, with the easy directions along the Fe [100] axes. Meanwhile, the negative H_4^s (the slope of the linear fitting) evidences the interfacial fourfold anisotropy at the Fe/MgO interfaces with the easy directions along the Fe [110] axes. The temperature dependence of H_4^s is presented in Fig. 4(f). The magnitude of H_4^s is enhanced at low temperature.

D. TMS and interfacial magnetic anisotropy

The positive H_4^b aligns the bulk Fe magnetization along the Fe [100] axes, while the negative H_4^s tends to tilt the interfacial Fe magnetization toward the Fe [110] axes [Fig. 5(a)], leading to the Fe magnetization reorientation and the nonuniform magnetization states at the Fe/MgO interfaces. Here, H_4^s is

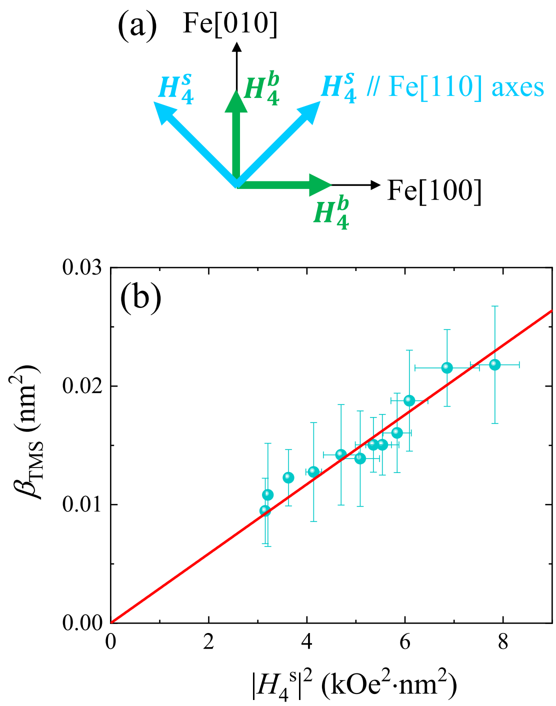

FIG. 5. (a) Schematic of H_4^b and H_4^s. The presence of H_4^s causes the Fe magnetization reorientation at the Fe/MgO interfaces. (b) The linear dependence of β_{TMS} on $|H_4^s|^2$, illustrating the dominant role of H_4^s on two-magnon scattering (TMS) damping.

competitive with H_{res}, so that the nonuniform magnetization states persist at FMR and result in a nonuniform magnetization precession at resonance (i.e., the short wavelength magnons). Interfacial magnetic anisotropy shifts the energy dispersion of the magnons (standing spin wave) with the wave vector normal to the film interface, resulting in the short wavelength magnon mode which is degenerate with FMR mode in frequency. Energy dissipation occurs in the manner of the unconserving magnon scattering between two degenerate modes (referred to as TMS), as well as the relaxation of the dephasing character [10]. Therefore, interfacial magnetic anisotropy plays a key role in the TMS process, i.e., an extrinsic damping mechanism.

Hence, it is conceivable that the enhanced H_4^s at low temperature [Fig. 4(f)] could induce an increase of TMS damping, which is observed in Fig. 3(d). Figure 5(b) presents a linear dependence of β_{TMS} on $|H_4^s|2$, illustrating the correlation between TMS damping and the interfacial fourfold anisotropy H_4^s [11,21]. In this regard, Gilbert damping could be reduced by optimizing the interface, e.g., the α_{TMS} of Fe/Pd is much smaller than that of Fe/Cu [29]. The inhomogeneous magnetization states at the interfaces might play the same role of the scattering centers [22], contributing to TMS damping, which could be suppressed by the external magnetic field. Therefore, a sufficiently strong magnetic field or FMR mode at sufficiently high frequency (i.e., large wave vector) can help to suppress TMS damping as well [18]. Additionally, single-crystalline films may provide the lower TMS damping with respect to polycrystalline films, due to the much lower density of scattering centers in the bulk of films.

IV. SUMMARY

In summary, intrinsic and extrinsic Gilbert damping of Fe thin films are disentangled via thickness-dependent α_G measurements. An enhanced α_G at low temperature is observed, which is attributed to both intrinsic Gilbert and TMS damping. Intrinsic Gilbert damping is found to be governed by the intraband transition at low temperature, as well as by the interband transition close to room temperature. Meanwhile, the in-plane fourfold anisotropy of Fe films is determined quantitatively with thickness and temperature dependence. The correlation between the interfacial fourfold anisotropy and TMS damping is revealed as well. Our result manifests the thickness-dependent α_G measurement as a universal and effective method to quantitatively disentangle the various damping mechanisms.

ACKNOWLEDGMENTS

This paper is supported by the National Key Research and Development Program of China (No. 2017YFA0303303) and the National Natural Science Foundation of China (No. 11874072).

[1] T. L. Gilbert, Phys. Rev. **100**, 1243 (1955).
[2] A. V. Chumak, V. I. Vasyuchka, A. A. Serga, and B. Hillebrands, Nature Phys. **11**, 453 (2015).
[3] M. A. W. Schoen, D. Thonig, M. L. Schneider, T. J. Silva, H. T. Nembach, O. Eriksson, O. Karis, and J. M. Shaw, Nature Phys. **12**, 839 (2016).
[4] A. J. Lee, J. T. Brangham, Y. Cheng, S. P. White, W. T. Ruane, B. D. Esser, D. W. McComb, P. C. Hammel, and F. Yang, Nature Commun. **8**, 234 (2017).
[5] V. Kamberský, Czech. J. Phys. B **26**, 1366 (1976).
[6] K. Gilmore, Y. U. Idzerda, and M. D. Stiles, Phys. Rev. Lett. **99**, 027204 (2007).
[7] A. Brataas, Y. Tserkovnyak, and G. E. W. Bauer, Phys. Rev. Lett. **101**, 037207 (2008).
[8] P. He, X. Ma, J. W. Zhang, H. B. Zhao, G. Lüpke, Z. Shi, and S. M. Zhou, Phys. Rev. Lett. **110**, 077203 (2013).
[9] B. Khodadadi, A. Rai, A. Sapkota, A. Srivastava, B. Nepal, Y. Lim, D. A. Smith, C. Mewes, S. Budhathoki, A. J. Hauser, M. Gao, J.-F. Li, D. D. Viehland, Z. Jiang, J. J. Heremans, P. V. Balachandran, T. Mewes, and S. Emori, Phys. Rev. Lett. **124**, 157201 (2020).
[10] R. Arias and D. L. Mills, Phys. Rev. B **60**, 7395 (1999).
[11] A. Azevedo, A. B. Oliveira, F. M. de Aguiar, and S. M. Rezende, Phys. Rev. B **62**, 5331 (2000).
[12] J. M. Lock, Br. J. Appl. Phys. **17**, 1645 (1966).
[13] C. Scheck, L. Cheng, and W. E. Bailey, Appl. Phys. Lett. **88**, 252510 (2006).

[14] M. A. W. Schoen, J. M. Shaw, H. T. Nembach, M. Weiler, and T. J. Silva, Phys. Rev. B **92**, 184417 (2015).
[15] K. Chen and S. Zhang, Phys. Rev. Lett. **114**, 126602 (2015).
[16] A. Conca, S. Keller, M. R. Schweizer, E. Th. Papaioannou, and B. Hillebrands, Phys. Rev. B **98**, 214439 (2018).
[17] L. Chen, S. Mankovsky, S. Wimmer, M. A. W. Schoen, H. S. Körner, M. Kronseder, D. Schuh, D. Bougeard, H. Ebert, D. Weiss, and C. H. Back, Nature Phys. **14**, 490 (2018).
[18] W. K. Peria, T. A. Peterson, A. P. McFadden, T. Qu, C. Liu, C. J. Palmstrøm, and P. A. Crowell, Phys. Rev. B **101**, 134430 (2020).
[19] S. Ingvarsson, L. Ritchie, X. Y. Liu, Gang Xiao, J. C. Slonczewski, P. L. Trouilloud, and R. H. Koch, Phys. Rev. B **66**, 214416 (2002).
[20] A. Ruiz-Calaforra, T. Brächer, V. Lauer, P. Pirro, B. Heinz, M. Geilen, A. V. Chumak, A. Conca, B. Leven, and B. Hillebrands, J. Appl. Phys. **117**, 163901 (2015).
[21] L. Zhu, D. C. Ralph, and R. A. Buhrman, Phys. Rev. Lett. **123**, 057203 (2019).
[22] Y. Li and W. E. Bailey, Phys. Rev. Lett. **116**, 117602 (2016).
[23] R. Meckenstock, D. Spoddig, Z. Frait, V. Kambersky, and J. Pelzl, J. Magn. Magn. Mater. **272–276**, 1203 (2004).
[24] S. Sakamoto, T. Higo, S. Tamaru, H. Kubota, K. Yakushiji, S. Nakatsuji, and S. Miwa, Phys. Rev. B **103**, 165122 (2021).
[25] W. N. Cao, J. Li, G. Chen, J. Zhu, C. R. Hu, and Y. Z. Wu, Appl. Phys. Lett. **98**, 262506 (2011).
[26] J. Li, E. Jin, H. Son, A. Tan, W. N. Cao, C. Hwang, and Z. Q. Qiu, Rev. Sci. Instrum. **83**, 033906 (2012).
[27] N. Naftalis, A. Kaplan, M. Schultz, C. A. F. Vaz, J. A. Moyer, C. H. Ahn, and L. Klein, Phys. Rev. B **84**, 094441 (2011).
[28] J. Li, Y. Meng, J. S. Park, C. A. Jenkins, E. Arenholz, A. Scholl, A. Tan, H. Son, H. W. Zhao, C. Hwang, Y. Z. Wu, and Z. Q. Qiu, Phys. Rev. B **84**, 094447 (2011).
[29] Y. Li, Y. Li, Q. Liu, Z. K. Xie, E. Vetter, Z. Yuan, W. He, H. L. Liu, D. L. Sun, K. Xia, W. Yu, Y. B. Sun, J. J. Zhao, X. Q. Zhang, and Z. H. Cheng, New J. Phys. **21**, 103040 (2019).